Inorganic Chemistry

ARTICLE

pubs.acs.org/IC

Development of Bifunctional Stilbene Derivatives for Targeting and Modulating Metal-Amyloid-β Species

Joseph J. Braymer,[†] Jung-Suk Choi,[‡] Alaina S. DeToma,[†] Chen Wang,[†] Kisoo Nam,[‡] Jeffrey W. Kampf,[†] Ayyalusamy Ramamoorthy,[†,§] and Mi Hee Lim*[,†,‡]

[†]Department of Chemistry, [‡]Life Sciences Institute, and [§]Biophysics, University of Michigan, Ann Arbor, Michigan 48109, United States

Supporting Information

ABSTRACT: Amyloid-β (Aβ) peptides and their metal-associated aggregated states have been implicated in the pathogenesis of Alzheimer's disease (AD). Although the etiology of AD remains uncertain, understanding the role of metal-Aβ species could provide insights into the onset and development of the disease. To unravel this, bifunctional small molecules that can specifically target and modulate metal-Aβ species have been developed, which could serve as suitable chemical tools for investigating metal-Aβ-associated events in AD. Through a rational structure-based design principle involving the incorporation of a metal binding site into the structure of an Aβ interacting molecule, we devised stilbene derivatives (**L1-a** and **L1-b**) and demonstrated their reactivity toward metal-Aβ species. In particular, the dual functions of compounds with different structural features (e.g., with or without a dimethylamino group) were explored by UV−vis, X-ray crystallography, high-resolution 2D NMR, and docking studies. Enhanced bifunctionality of compounds provided greater effects on metal-induced Aβ aggregation and neurotoxicity in vitro and in living cells. Mechanistic investigations of the reaction of **L1-a** and **L1-b** with Zn^{2+}-Aβ species by UV−vis and 2D NMR suggest that metal chelation with ligand and/or metal−ligand interaction with the Aβ peptide may be driving factors for the observed modulation of metal-Aβ aggregation pathways. Overall, the studies presented herein demonstrate the importance of a structure-interaction-reactivity relationship for designing small molecules to target metal-Aβ species allowing for the modulation of metal-induced Aβ reactivity and neurotoxicity.

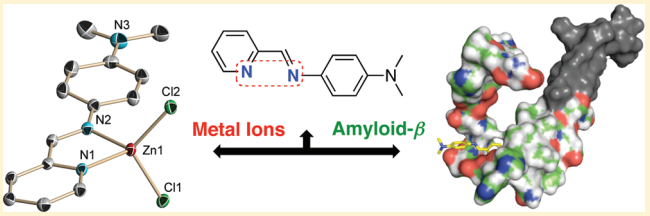

INTRODUCTION

Alzheimer's disease (AD) is a serious form of dementia that causes deterioration of cognitive function in over 5.3 million people in the United States.[1,2] One current hypothesis of the underlying causes of AD involves the accumulation of plaques composed of aggregated amyloid-β (Aβ) peptides in the brain.[2−5] Cleavage of the transmembrane amyloid precursor protein (APP) by β- and γ-secretases results in the production of Aβ, which contains 38−43 amino acid residues. Through hydrophobic interactions, Aβ monomers in solution can self-assemble to form aggregated states (e.g., oligomers, protofibrils, and fibrils).[2,5−7] While the fibril-containing plaques can be identified in the brain of AD patients, how these peptides and their possible aggregation states are connected to AD is not completely understood. Current evidence suggests that Aβ monomers are relatively nontoxic while aggregated Aβ species (in particular, soluble low molecular weight (MW) Aβ species, including dimers) are shown to be toxic to neuronal cells and therefore may lead to AD neuropathogenesis; however, their relation to AD development remains obscure.[2−4,6]

In Aβ plaques, concentrated areas of metal ions such as Fe, Cu, and Zn have been observed.[5,8−15] These metal ions are known to facilitate Aβ aggregation upon binding to the Aβ peptide (via three histidine residues, H6, H13, and H14).[5,10,11,13−20] Additionally, reactive oxygen species (ROS) can be generated by the redox cycling of Cu bound to Aβ, which may be responsible for the neurotoxicity of the disease.[2,10−17,21−25] These characteristics indicate that metal ions are able to influence pathways of Aβ aggregation and neurotoxicity, but the molecular mechanisms of metal-Aβ-associated events are not fully understood.

Previous studies have shown that metal chelators such as 2,2′,2″,2‴-(ethane-1,2-diyldinitrilo)tetraacetic acid (EDTA), bathocuproine, desferrioxamine, and clioquinol (CQ) are capable of reducing metal-mediated Aβ aggregation and neurotoxicity.[2,10−12,15−17,21,22,24−32] Use of these metal chelating agents to understand the details of metal-Aβ chemistry and biology is limited because they may not be specific for metal-Aβ species in vivo. This may be due to the lack of Aβ interaction functionality that could hinder metal chelators from targeting metal ions associated with Aβ species in heterogeneous environments. There have been recent efforts to rationally design small molecules that can target metal-Aβ species and modulate their aggregation pathways by appending metal chelation sites onto known Aβ imaging agents.[5,15,33−39] Some of these compounds have truncated Aβ-interaction moieties and/or nonspecific metal binding properties, which might hamper their capability to target and interact specifically with metal-Aβ species in vitro and in vivo. To improve this, we have constructed bifunctional small molecules via the direct incorporation of a metal binding site into the scaffold of previously reported Aβ interacting

Received: June 7, 2011
Published: September 28, 2011

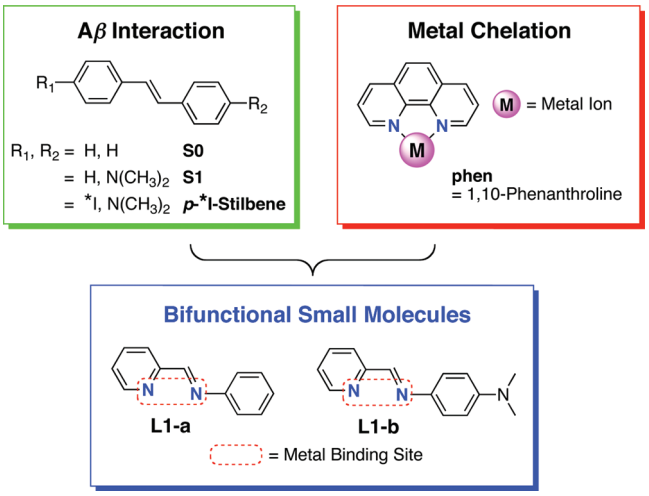

Figure 1. Rational structure-based design strategy for bifunctional small molecules. Incorporation of a metal binding site into an Aβ interacting molecule is the design basis for **L1-a** and **L1-b**. **L1-a** = *N*-(pyridin-2-ylmethylene)aniline; **L1-b** = N^1,N^1-dimethyl-N^4-(pyridin-2-ylmethylene)-benzene-1,4-diamine; **S0** = (*E*)-1,2-diphenylethene; **S1** = *N*,*N*-dimethyl-4-(2-phenylethenyl)benzamine. *I = ^{123}I or ^{125}I.

molecules without major structural modification (the rational structure-based design).[33,34,37−39] Our first-generation compound (**L1-b**) was devised by applying this synthetic design strategy employing the structure of an Aβ imaging agent, *p*-$^{123/125}$I-stilbene (Figure 1).[37] Our small molecule showed bifunctionality (metal chelation and Aβ interaction) as well as control of Cu^{2+}-induced Aβ aggregation processes and neurotoxicity in vitro and in living cells.[37] In addition, our recent studies using other bifunctional small molecules suggest that chemical structural moieties such as the dimethylamino functionality are important to tune their reactivity toward metal-induced Aβ aggregation and neurotoxicity.[38] To understand a structure-interaction-reactivity relationship of the stilbene framework, we report herein the studies of metal binding and Aβ interaction of **L1-a** (the compound that does not contain a dimethylamino group, Figure 1) and **L1-b**, the effects on the modulation of metal (Cu^{2+} or Zn^{2+})-mediated Aβ aggregation and Cu-Aβ-induced ROS production in vitro, as well as the influence on metal-Aβ neurotoxicity in living cells. Furthermore, Aβ interaction of **L1-a** and **L1-b** was compared to that of **S0** and **S1** that have the stilbene scaffold without a metal coordination site (a structure-interaction relationship). Our current findings demonstrate that slight difference in chemical structures of small molecules is able to influence their Aβ interaction, which can improve reactivity toward metal-Aβ species.

EXPERIMENTAL SECTION

Materials and Procedures. All reagents were purchased from commercial suppliers and used as received unless stated otherwise. The compound **L1-b** was synthesized by the previous method.[37] Aβ_{1-40} peptide (free acid terminal) was purchased from EZBiolab (>95% purity, Carmel, IN) or rPeptide (>97% purity, Athens, GA). The amino acid sequence for the Aβ_{1-40} peptide is DAEFRHDSGYEVHHQKLVFFAEDVGSNKGAIIGLMVGGVV. The hydrogen peroxide (H_2O_2) assay using horseradish peroxidase (HRP, Sigma, St. Louis, MO) and Amplex Red (AnaSpec, Inc., Fremont, CA) was performed following previously published procedures.[23,32,37,38,40] The metal ion selectivity of **L1-b** was determined in EtOH with metal chloride salts ($MgCl_2$, $CaCl_2$, $MnCl_2$, $FeCl_2$, $FeCl_3$, $CoCl_2$, $NiCl_2$, and $ZnCl_2$) using UV−vis according to the previously published report.[38] All stock solutions of metal salts were prepared in EtOH. Studies employing $FeCl_2$ were conducted anaerobically. The selectivity values (A_M/A_{Cu}, Supporting Information, Figure S2) were obtained by comparing the absorbance of the solution at 525 nm before and after the addition of $CuCl_2$. Absorption values were normalized relative to that of **L1-b** and $CuCl_2$ at this wavelength (525 nm) to provide minimal interference between absorption bands. NMR and IR spectra of small molecules were recorded on a 400 MHz Varian NMR spectrometer and on a Perkin-Elmer Spectrum BX FT-IR instrument, respectively. The NMR investigations of the interaction of compounds with Aβ were conducted using a 900 MHz Bruker Avance spectrometer (Michigan State University). Optical spectra were collected on an Agilent 8453 UV−vis spectrophotometer. Mass spectrometric measurements were performed using a Micromass LCT Electrospray Time-of-Flight mass spectrometer. A SpectraMax M5 microplate reader (Molecular Devices) was used for measurements of absorbance for the cell viability assay and fluorescence for the H_2O_2 assay.

[Zn(L1-a)Cl$_2$]. Colorless plate crystals were grown by vapor diffusion of diethyl ether (Et_2O) into an acetonitrile (CH_3CN) solution of commercially available **L1-a** (5.0 mg, 27 μmol) and $ZnCl_2$ (3.7 mg, 27 μmol) at room temperature over 2 days. The crystals were isolated, washed with Et_2O three times, and dried in vacuo (7.1 mg, 22 μmol, 81%). FTIR (KBr, cm^{-1}): 3445 (w, br), 3086 (vw, sh), 3085 (vw), 3064 (w), 3024 (w), 1620 (vw, sh), 1594 (s), 1563 (w), 1494 (s), 1476 (m, sh), 1456 (m, sh), 1445 (s), 1421 (vw, sh), 1385 (vw, sh), 1368 (m), 1339 (vw), 1303 (w), 1280 (w), 1236 (w), 1195 (w), 1186 (vw, sh), 1158 (w), 1111 (m), 1076 (vw), 1050 (w), 1024 (s), 1000 (vw, sh), 976 (w), 959 (w), 916 (m), 840 (vw), 778 (vs), 740 (s), 684 (s), 650 (m), 616 (vw, sh), 567 (w), 535 (m), 481 (vw), 462 (vw, sh), 413 (w). ^{1}H NMR (400 MHz, CD_3CN): δ = 7.54 (t, *J* = 8 Hz, 1H), 7.61 (t, *J* = 8 Hz, 2H), 7.80 (d, *J* = 8 Hz, 2H), 7.94 (t, *J* = 8 Hz, 1H), 8.16 (d, *J* = 8 Hz, 1H), 8.36 (t, *J* = 8 Hz, 1H), 8.85 (d, *J* = 8 Hz, 1H), 9.03 (s, 1H). ESI(+)MS (*m*/*z*): $[M\text{-}Cl]^+$ calcd for $C_{12}H_{10}ClN_2Zn$, 281.0, found 280.9. Anal. Calcd for $C_{12}H_{10}Cl_2N_2Zn$: C, 45.25; H, 3.16; N, 8.80. Found: C, 45.24; H, 3.17; N, 8.70. UV−vis [CH_3CN; λ/nm ($\varepsilon \times 10^4$, M^{-1} cm^{-1})]: 235 (1.1), 241 (1.2), 328 (1.9), 341 (1.8).

[Zn(L1-b)Cl$_2$]. Orange needle crystals were grown by vapor diffusion of Et_2O into a CH_3CN solution of **L1-b** (5.0 mg, 22 μmol) and $ZnCl_2$ (3.0 mg, 22 μmol) at room temperature overnight. The crystals were isolated, washed with Et_2O three times, and dried in vacuo (6.8 mg, 19 μmol, 86%). FTIR (KBr, cm^{-1}): 3440 (w, br), 3077 (vw), 3027 (vw), 3008 (vw), 2974 (vw), 2902 (w), 2863 (vw, sh), 2822 (vw), 1622 (s), 1599 (vs), 1583 (s, sh), 1546 (vs), 1471 (s), 1447 (s), 1415 (vw, sh), 1371 (s), 1328 (vw), 1321 (vw), 1300 (w), 1284 (w), 1250 (w), 1231 (w), 1215 (vw, sh), 1188 (s), 1173 (s), 1159 (s, sh), 1123 (vw, sh), 1105 (vw), 1067 (w), 1050 (vw), 1024 (vw), 1000 (vw), 946 (w), 923 (vw, sh), 842 (vw, sh), 810 (s), 771 (m), 744 (w), 644 (vw, sh), 642 (w), 551 (vw), 529 (m), 430 (vw), 411 (w). ^{1}H NMR (400 MHz, CD_3CN): δ = 3.06 (s, 6H), 6.86 (d, *J* = 8 Hz, 2H), 7.71 (d, *J* = 8 Hz, 2H), 7.80 (t, *J* = 4 Hz, 1H), 8.00 (d, *J* = 8 Hz, 1H), 8.27 (t, *J* = 8 Hz, 1H), 8.75 (d, *J* = 4 Hz, 1H), 8.86 (s, 1H). ESI(+)MS (*m*/*z*): $[M+H]^+$ Calcd for $C_{14}H_{16}Cl_2N_3Zn$, 360.0, found 360.0. Anal. Calcd for $C_{14}H_{15}Cl_2N_3Zn$: C, 46.50; H, 4.18; N, 11.62. Found: C, 46.44; H, 4.14; N, 11.57. UV−vis [CH_3CN; λ/nm ($\varepsilon \times 10^4$, M^{-1} cm^{-1})]: 277 (2.0), 477 (3.3).

X-ray Crystallographic Study. Single crystals suitable for data collection were mounted on a Bruker SMART APEX CCD-based X-ray diffractometer equipped with a low temperature device and fine focus Mo-target X-ray tube (λ = 0.71073 Å) operated at 1500 W power (50 kV, 30 mA). The X-ray intensities were measured at 85(2) K. Empirical absorption corrections were calculated with the SADABS or TWINABS program.[41] Structures were solved and refined with the SAINTPLUS and SHELXTL software packages.[42,43] All non-hydrogen

atoms were refined anisotropically. Hydrogen atoms were assigned in idealized positions, and each was given a thermal parameter equivalent to 1.2 times the thermal parameter of the atom to which it was attached. The structure solution was checked for higher symmetry with PLATON.[44] The highest electron density in the final difference Fourier maps for [**Zn(L1-a)Cl$_2$**] and [**Zn(L1-b)Cl$_2$**] were 1.181 and 1.112 e/Å^3, respectively, in the vicinity of the Zn center. In the structure of [**Zn(L1-b)Cl$_2$**], indexing performed using the CELL_NOW program[45] indicated that the crystal was a two-component, nonmerohedral twin. The data were processed with TWINABS and corrected for absorption.[41] The domains are related by a rotation of 179.8 degrees about the direct and reciprocal [0 1 0] axis. For this refinement, single reflections from component one as well as composite reflections containing a contribution from this component were used. Merging of the data was performed in TWINABS, and an HKLF 5 format file was used for refinement.

Two-Dimensional (2D) ^{1}H-^{15}N Transverse Relaxation Optimized Spectroscopy (TROSY)-Heteronuclear Single Quantum Correlation (HSQC) NMR Measurements. The ^{15}N-labeled Aβ_{1-40} was purchased from rPeptide and stored at −80 °C. Aβ (ca. 0.25 mg) was dissolved into a buffered solution containing sodium dodecyl-d_{25} sulfate (SDS-d_{25}, 200 mM), sodium phosphate buffer (20 mM, pH 7.3), and D_2O (7%, v/v) and was briefly vortexed.[37−39] The peptide solution was transferred to a Shigemi NMR tube. After acquiring spectra of the peptide, about 10 equiv (stock solutions: 5 mM in above buffer solution) of either **L1-a** or **L1-b** were added to the NMR samples of Aβ (ca. 190 μM Aβ). Control samples were conducted under similar conditions with the addition of 2.28 μL of either neat dimethyl sulfoxide-d_6 (DMSO-d_6) or a 50 mM DMSO-d_6 stock solution of **S0** or **S1** to a 300 μL solution containing 190 μM Aβ.[46] For NMR studies with Zn^{2+}, about 1.0 equiv of $ZnCl_2$ (0.57 μL of 100 mM stock solution in D_2O) was added into the peptide solution followed by treatment with 10 equiv of **L1-a** or **L1-b**. For the [Aβ + $ZnCl_2$ + **L1-a** or **L1-b**] solution, no further spectral changes were observed after 1 h of incubation. For NMR studies, the TROSY version of 2D ^{1}H-^{15}N HSQC spectra were recorded on the 900 MHz Bruker Avance NMR spectrometer (equipped with a TCI cryoprobe accessory) with 14.3 kHz and 1.7 kHz spectral width and 2048 and 128 complex data points in the ^{1}H and ^{15}N dimension, respectively, 4 scans for each t_1 experiment and 1.5 s recycle delay; each spectrum took 10 min for completion. The water ^{1}H peak was referenced to 4.78 ppm at 25 °C. ^{1}H-^{15}N HSQC peaks were assigned by comparison of the observed chemical shift values with those reported in the literature.[47] Combined ^{1}H and ^{15}N 2D chemicals shifts ($\Delta\delta_{N-H}$) were calculated from eq 1.[48−50] The 2D data were processed using Topspin software (version 2.1 from Bruker) and analyzed with Sparky (version 3.112).

$$\Delta\delta_{N\text{-}H} = \sqrt{\frac{(\Delta\delta_H)^2 + (0.2(\Delta\delta_N))^2}{2}} \quad (1)$$

Docking Studies of Compounds with AutoDock4. Docking of **L1-a**, **L1-b**, **S0**, and **S1** with the Aβ monomer was determined using the computational package AutoDock4 and AutoDockTools4 following previous reports.[38,51−53] The optimized structures of compounds were generated for AutoDockTools4 by the MMFF94 energy minimization in ChemBio3D Ultra 12.0. Ten peptide conformations from a previously determined NMR structure of Aβ_{1-40} monomer in SDS micelles (PDB 1BA4) were employed.[54] Of these conformations, five were in agreement with the NMR data and are depicted in Figure 4 and Supporting Information, Figure S4. The structural files of compounds and peptides were transferred to AutoDockTools4 and prepared for AutoGrid4 using a grid volume encompassing the entire peptide with 0.375 Å spacing: [Conformation: box size (Å): center (x,y,z)] A: 126 × 84 × 56: 7.663, 7.889, −8.706; B: 126 × 72 × 66: 0.194, −6.01, −7.711; C: 126 × 72 × 58: 5.665, −5.79, −8.124; D: 126 × 72 × 76: 5.432, −4.614, −12.983; E: 118 × 88 × 54: 10.202, 9.338, −4.058. In AutoDock4, each compound was evaluated with 256 Lamarckian genetic algorithm local searches (GALS) by a population size of 150 and 2.5 million energy evaluations. Additional default parameters remained unchanged unless otherwise specified. Conformations of compounds were analyzed by clusters in AutoDockTools4. The highest frequency and lowest energy conformation was chosen and portrayed docked to Aβ using Pymol.

Amyloid-β (Aβ) Peptide Experiments. Aβ_{1-40} peptide (1 mg, EZBiolab) was purchased, dissolved with ammonium hydroxide (1% v/v, aq), aliquoted to 10 samples, lyophilized, and stored at −80 °C. The stock solution (ca. 200 μM) for the reactions was made by redissolving Aβ with NH_4OH (1% v/v, aq, 10 μL) followed by dilution with ddH_2O or a buffer solution. Preparation of all Aβ samples followed the previously reported procedures.[37−39,55−58] The ddH_2O and buffer solutions used for Aβ experiments were treated with Chelex overnight to remove traces of metal ions. For the inhibition study, solutions of samples contained Aβ (25 μM), a metal chloride salt ($CuCl_2$ or $ZnCl_2$, 25 μM), and a compound (50 μM, stock solutions in DMSO, 1% v/v final DMSO concentration). The solutions were incubated for 24 h at 37 °C with constant agitation and analyzed by transmission electron microscopy (TEM) and Western blotting using an anti-Aβ antibody (6E10). For the disaggregation study, Aβ (25 μM) and a metal chloride salt ($CuCl_2$ or $ZnCl_2$, 25 μM) were incubated for 24 h at 37 °C with constant agitation. Afterward, a compound (50 μM, stock solutions in DMSO, 1% v/v final DMSO concentration) was added and incubated for 24 h at 37 °C with constant agitation. Buffered solutions (20 μM HEPES (2-[4-(2-hydroxyethyl)piperazin-1-yl]ethanesulfonic acid), pH 6.6 (for $CuCl_2$) or pH 7.4 (for $ZnCl_2$), 150 μM NaCl) were used for both studies.

Transmission Electron Microscopy (TEM). Samples for TEM were prepared by following the previously reported methods.[37−39,55−58] Glow-discharged grids (Formar/Carbon 300-mesh, Electron Microscopy Sciences) were treated with Aβ aggregated samples (5 μL, 25 μM) for 2 min at room temperature. Excess sample was removed using filter paper followed by washing twice with ddH_2O. Each grid incubated with uranyl acetate (1% w/v, ddH_2O, 5 μL, 1 min) was blotted and dried for 15 min at room temperature. Images from each sample were taken by a Philips CM-100 transmission electron microscope (80 kV, 25,000× magnification).

Native Gel Electrophoresis and Western Blotting. The reactions described above (Aβ Peptide Experiments) were visualized by native gel electrophoresis followed by Western blotting using an anti-Aβ antibody (6E10).[37−39,57,58] Each sample (10 μL, 25 μM) was separated on a 10−20% gradient Tris-tricine gel (Invitrogen). The gel was transferred onto a nitrocellulose membrane, blocked with bovine serum albumin (BSA, 3% w/v) in Tris-buffered saline (TBS) containing 0.1% Tween-20 (TBS-T) for 3 h at ambient temperature, and then incubated with an anti-Aβ antibody (6E10, 1:2,000) in 2% BSA in TBS-T for 3 h at ambient temperature. The membrane was probed with the horseradish peroxidase-conjugated goat antimouse antibody (1:10,000) in 2% BSA in TBS-T for 1 h at ambient temperature. The Thermo Scientific Supersignal West Pico Chemiluminescent Substrate was used to visualize protein bands.

Cytotoxicity (MTT Assay). Two human neuroblastoma SK-N-BE(2)-M17 (M17) and SK-N-AS (AS) cell lines were purchased from the American Type Culture Collection (ATCC). The M17 and AS cell lines were maintained in [1:1 Minimum Essential Media (MEM) and Ham's F12K Kaighn's Modification Media (F12K)] and [Dulbecco's Modified Eagle Medium (DMEM)] (GIBCO), respectively, containing 10% (v/v) fetal bovine serum (FBS, Atlanta Biologicals), 100 U/mL penicillin, and 100 mg/mL streptomycin (Invitrogen). The cells were grown at 37 °C in a humidified atmosphere of 5% CO_2. For the MTT (3-(4,5-dimethylthiazol-2-yl)-2,5-diphenyltetrazolium bromide, Sigma-Aldrich) assay, M17/AS cells were seeded in a 96 well plate

(for cytotoxicity studies of compounds without and with metal ions, 16,000/8,000 and 10,000/5,000 cells (in 100 μL per well) for 24 and 72 h experiments, respectively; for the investigations of regulating metal-Aβ neurotoxicity by compounds, 16,000 M17 cells (in 100 μL per well)).[37,38,58] After 24 h, cells were treated with [compounds with or without metal ions] and [Aβ, $CuCl_2$ or $ZnCl_2$, and/or compounds]. The final concentration of DMSO in each well was fixed to 1%. Then, the cells were incubated for 24 or 72 h at 37 °C. After the incubation, the cells were treated with 25 μL MTT (5 mg/mL in PBS) for 4 h at 37 °C and then were lysed in a buffered solution containing *N*,*N*-dimethylformamide (pH 4.5, 50% (aq, v/v)) and SDS (20% (w/v)) overnight at room temperature in the dark. The absorbance (A_{600}) was measured using a microplate reader.

RESULTS AND DISCUSSION

Design Consideration and Preparation of Bifunctional Small Molecules for Targeting and Modulating Metal-Aβ Species. To elucidate the mechanisms of metal-induced Aβ aggregation and neurotoxicity in AD, chemical tools that can specifically target and regulate metal-Aβ species are needed. We have designed bifunctional chemical reagents that contain a metal binding site in the structure of Aβ interaction molecules.[33,34,37−39] In particular, we have focused on the incorporation of a metal chelation moiety into the stilbene framework (Aβ imaging agent) for bifunctionality (metal chelation and Aβ interaction) (Figure 1).

Recently, we reported that **L1-b**, in which two nitrogen donor atoms were introduced into the stilbene scaffold for metal binding (Figure 1), exhibited bifunctionality and an ability to modulate Cu^{2+}-induced Aβ events such as aggregation and neurotoxicity in vitro and in living cells.[37] Moreover, amine derivatives of **L1-a** and **L1-b** have been prepared for this purpose indicating promising applications in biological systems.[38] From this and other studies, the dimethylamino functionality in the small molecules has been suggested to be an important structural moiety for Aβ interaction.[38,59,60] To understand the structure-interaction-reactivity relationship, **L1-a** (that does not have a dimethylamino group) was studied along with **L1-b** (vide infra). The compounds **L1-a** (commercially available) and **L1-b** can be synthesized in high yield (>90%) through Schiff base condensation of an aldehyde and primary amine following previously established methods.[37,61]

Metal Binding Properties of L1-a and L1-b. Following our rational structure-based design principle, two nitrogen atom donors were introduced into the stilbene framework to generate a metal chelation site (Figure 1). To elucidate metal binding properties of our compounds, the reactions of the compounds with metal chloride salts in solution were evaluated using UV−vis and the metal complexes [**Zn(L1-a)Cl$_2$**] and [**Zn(L1-b)Cl$_2$**] were isolated and characterized by X-ray crystallography. First, metal coordination was observed by the shifts in the optical bands of our compounds upon addition of $CuCl_2$ or $ZnCl_2$ in EtOH (Table 1 and Supporting Information, Figure S1). Modest changes in the absorption spectra were shown for **L1-a** with 1 equiv of $CuCl_2$ or $ZnCl_2$ whereas both metal chloride salts caused noticeable changes in the spectra of **L1-b**. The ligand **L1-b** interacted with Cu^{2+} based on the new absorption bands at about 450 nm. The observed peaks from 470−480 nm that grew in upon the addition of $ZnCl_2$ indicated that **L1-b** could bind to Zn^{2+} as well. Furthermore, **L1-b** having the dimethylamino group presented more apparent changes in the optical spectra

Table 1. Summary of Optical Results[a]

	spectral properties (nm)			
compound	unbound[b]	$CuCl_2$[b]	$ZnCl_2$[b]	crystals[c]
L1-a	280, 323	297	283, 325	[**Zn(L1-a)Cl$_2$**] 235, 241, 328, 341
L1-b	316, 396	318, 445	403, 484 408,[d] 473[d]	[**Zn(L1-b)Cl$_2$**] 277, 475

[a] The optical spectra are depicted in Supporting Information, Figure S1. [b] Measurements were performed in EtOH at room temperature following 10 min incubation. Ratio of metal to ligand was 1:1 unless otherwise noted. [c] Optical data were obtained in CH_3CN. [d] [$ZnCl_2$]/[**L1-b**] = 10:1.

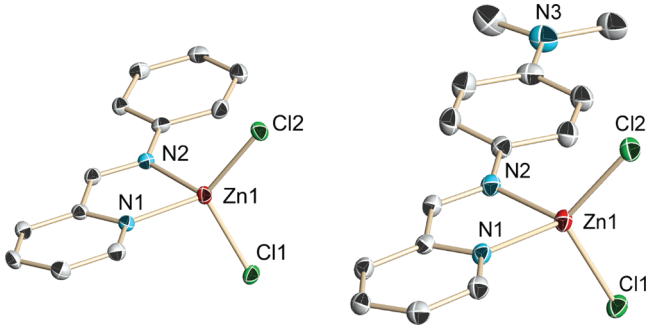

Figure 2. ORTEP diagrams of [**Zn(L1-a)Cl$_2$**] (left) and [**Zn(L1-b)Cl$_2$**] (right) showing 50% probability thermal ellipsoids. X-ray crystallographic data are summarized in Supporting Information, Table S1.

in the presence of metal chloride salts, compared to **L1-a** (Table 1 and Supporting Information, Figure S1). The optical features, indicative of the Zn^{2+}-**L1-a** or Zn^{2+}-**L1-b** interaction, were also shown in the solution of isolated metal complexes [**Zn(L1-a)Cl$_2$**] or [**Zn(L1-b)Cl$_2$**] (Figure 2, vide infra) in CH_3CN (Table 1 and Supporting Information, Figure S1). Thus, UV−vis studies described above suggest metal binding of **L1-a** and **L1-b** in solution. Additionally, the investigation for the metal selectivity of **L1-b** using UV−vis indicated that this ligand was relatively selective for Cu^{2+} over other metal ions such as Mg^{2+}, Ca^{2+}, Mn^{2+}, Fe^{2+}, Fe^{3+}, Co^{2+}, Ni^{2+}, and Zn^{2+} in EtOH (Supporting Information, Figure S2; [**L1-b**] = 40 μM, [$M^{2+/3+}$] = 40 μM, at room temperature). Because of the limited stability of these imine compounds in aqueous solutions,[62] further metal binding properties such as pH-variable solution speciation[36,38] were not studied.

To further understand the metal binding properties, X-ray quality single crystals of the metal complexes [**Zn(L1-a)Cl$_2$**] and [**Zn(L1-b)Cl$_2$**] (Figure 2) were grown by slow diffusion of Et_2O into a solution of ligand and $ZnCl_2$ (1:1) in CH_3CN. Crystallographic data and selected bond lengths and angles are summarized in Supporting Information, Tables S1 and S2, respectively. As depicted in Figure 2, the structures present that two nitrogen atoms of the ligands are responsible for metal chelation. The overall conformation of the imine ligands **L1-a** and **L1-b** of the Zn complexes exhibited planarity in the solid state, with distorted tetrahedral geometry around the metal center. The bond lengths and angles for the Zn complexes did not vary significantly depending on the presence of the dimethylamino group; however, the slight difference in bond angles and the Zn−N1 bond length between [**Zn(L1-a)Cl$_2$**] and

dx.doi.org/10.1021/ic2012205 |*Inorg. Chem.* 2011, 50, 10724–10734

[**Zn(L1-b)Cl$_2$**] was indicated (Table 2; e.g., Zn−N1 (Å) = 2.060(2) versus 2.0446(17), respectively). A Zn^{2+} complex with a structure similar to **L1-b** where the dimethylamino group is substituted with an iodine atom has been reported.[63] The molecule binds to $ZnCl_2$ in a 1:1 ratio to form a slightly distorted tetrahedral metal center with bond lengths and angles that are similar to those of [**Zn(L1-a)Cl$_2$**] and [**Zn(L1-b)Cl$_2$**]. This suggests that neither an electron withdrawing nor electron donating substituent in the *para* position of the phenyl ring significantly alters bond lengths or angles. Overall, X-ray crystal structure determination confirmed metal chelation by **L1-a** and **L1-b** via two nitrogen donor atoms.

Table 2. Selected Bond Lengths (Å) and Angles (deg)[a]

	[Zn(L1-a)Cl$_2$]	[Zn(L1-b)Cl$_2$]
Zn1−N1	2.060(2)	2.0446(17)
Zn1−N2	2.081(2)	2.0828(18)
Zn1−Cl1	2.2280(6)	2.2162(8)
Zn1−Cl2	2.1998(6)	2.2056(8)
N1−Zn1−N2	81.20(8)	82.24(7)
N1−Zn1−Cl1	107.72(6)	110.16(6)
N1−Zn1−Cl2	119.14(6)	117.42(6)
N2−Zn1−Cl1	111.40(6)	110.06(5)
N2−Zn1−Cl2	117.10(6)	120.03(6)
Cl1−Zn1−Cl2	115.48(2)	113.18(2)

[a] Numbers in parentheses are estimated standard deviations in the last significant figures. Atoms are labeled as indicated in Figure 2.

Aβ Interaction with L1-a, L1-b, S0, and S1. To establish the extent of interaction of **L1-a** and **L1-b** with Aβ in the absence of metal ions, which along with metal chelation affords bifunctionality, high-resolution 2D ^{1}H-^{15}N TROSY-HSQC NMR experiments were performed. SDS-d_{25} was employed in NMR studies of Aβ to solubilize the peptide and prevent its aggregation.[37−39,47,54,64] When bound to SDS micelles, the Aβ monomer adopts two α-helical segments involving residues Q15−N27 and G29−M35.[47,54] Helicity has also been observed in solution and when in contact with other biological molecules and has been suggested to precede the aggregation pathways of Aβ leading to proposed neurotoxic oligomers.[4,6,65−68] Thus, this system can provide an adequate model for determining the ability of our compounds to interact with and target a biologically relevant Aβ conformation. As a comparison of the interaction of our bifunctional molecules with Aβ, **S0** and **S1** that do not contain a metal binding site (Figure 1) were additionally investigated.

Changes in chemical shifts of Aβ were observed upon the addition of **L1-a** and **L1-b** (Figure 3, ca. 10 equiv, SDS-d_{25} (200 mM), sodium phosphate buffer (20 mM, pH 7.3), and D_2O (7%, v/v)), suggesting direct Aβ interaction with our small molecules. This experiment was carried out in the absence of dimethylsulfoxide (DMSO), which is different from the previous

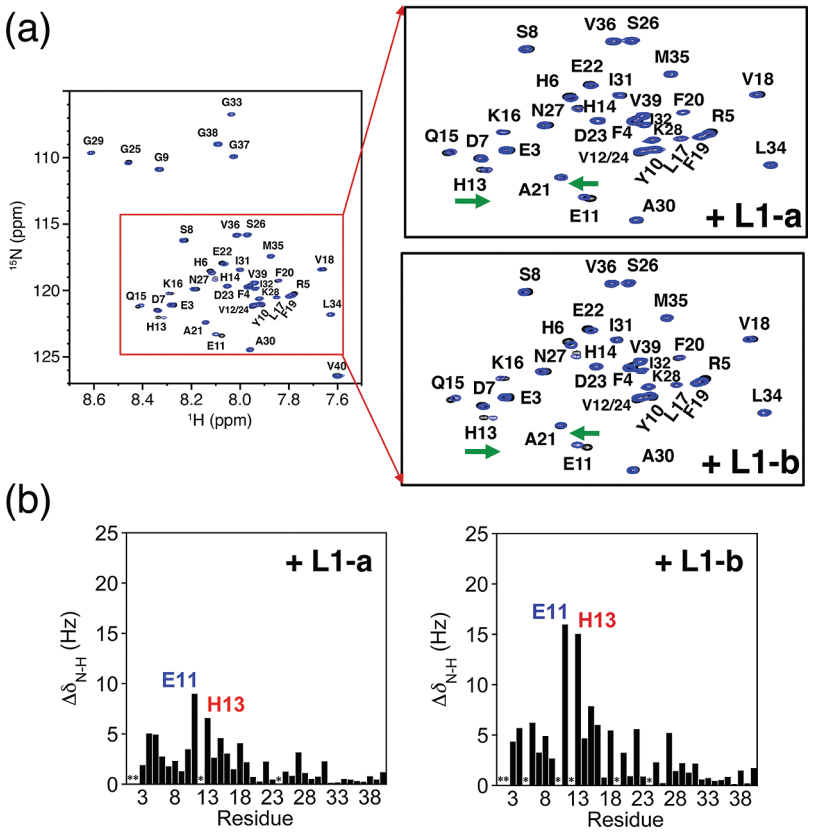

Figure 3. 2D ^{1}H-^{15}N TROSY-HSQC NMR study of the interaction of small molecules with ^{15}N-labeled Aβ$_{1-40}$ (900 MHz). (a) NMR spectra of the Aβ peptide (shown in black; ca. 308 μM in SDS-d_{25} (200 mM), sodium phosphate buffer (20 mM, pH 7.3, 7% D_2O (v/v), 25 °C)) and the peptide with the addition of 10 equiv of **L1-a** or **L1-b** shown in blue (full spectrum of **L1-b** is shown on the left). Green arrows indicate the direction of resonance shift. (b) Changes in combined ^{1}H and ^{15}N chemical shifts calculated from eq 1 upon the addition of 10 equiv of compounds to Aβ as a function of peptide sequence. * Denotes absent or overlapped signals. The amino acid sequence for the Aβ$_{1-40}$ peptide is DAEFRHDSGYEVHHQKLVFFAED-VGSNKGAIIGLMVGGVV.

dx.doi.org/10.1021/ic2012205 |*Inorg. Chem.* 2011, 50, 10724–10734

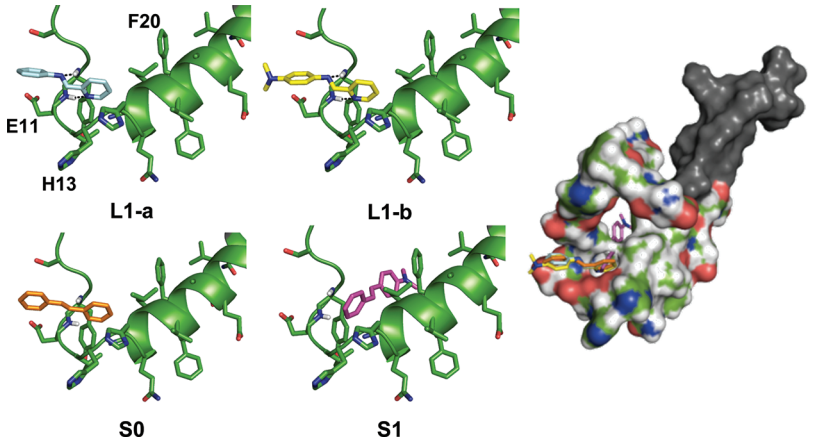

Figure 4. Possible conformations of **L1-a** (light blue), **L1-b** (yellow), **S0** (orange), and **S1** (magenta) docked with $A\beta_{1-40}$ (PDB 1BA4) by AutoDock4. The cartoon (left) and surface (right) versions of the peptide indicate interactions with compounds. The N-terminal and inner helix regions of $A\beta$ (D1−N27) are highlighted in color. Hydrogen bonding is indicated with dashed lines (1.9−2.2 Å).

report regarding the interaction of **L1-b** with $A\beta$ monomer.[37] Both compounds exerted an influence mainly on the N-terminal portion of the peptide (E3−Q15) where shifting occurred the most at residues E11 and H13. To understand the effect of the dimethylamino functionality on $A\beta$ interaction (**L1-a** versus **L1-b**), the chemical shift patterns were compared. While **L1-b** interacted more broadly through the N-terminal region and also with the inner helix of the peptide (Q15−N27), **L1-a** had fewer contacts in these portions of the peptide and did not show as strong of an interaction (Figure 3). For **L1-b**, a periodic trend occurred along the peptide backbone (Figure 3b), similar to our recently reported heterocyclic bifunctional IMPY derivative.[39] The shifting of residues Q15, V18, and E22 suggest that these residues may lie on a similar face of the inner helix (Q15−N27 depicted in Figure 4) and shift because of direct interaction with compound or a change in conformation upon ligand binding.[6,47,54] The absence of the dimethylamino structural moiety in **L1-a**, which has been proposed to be important in $A\beta$ interaction,[38,59,60] may explain why its degree of interaction with $A\beta$ is less than that of **L1-b**. Furthermore, the observation that the residues E11 and H13 were significantly shifted by our bifunctional molecules is important because these residues are near the proposed metal binding site of $A\beta$ (H6, H13, and H14).[5,10,11,13−15,18−20,22,40] Because of the close proximity of our compounds to the metal binding residues, it is possible that **L1-a** and **L1-b** may be able to target metal ions surrounded by $A\beta$ peptides.

To further compare the effect of both the addition of two nitrogen atoms and the presence of the dimethylamino group in our molecules, the compounds without a metal binding site, **S0** and **S1**, were also studied by NMR. Because of the low solubility of **S0** and **S1** in the buffered conditions above, DMSO was employed to deliver the compounds to the $A\beta$ solution.[46] Both compounds and DMSO alone (ca. 2 equiv of compound) appeared to have an influence on the shifting of residues but shifting trends were different from **L1-a** and **L1-b** (Supporting Information, Figure S3). Upon addition of both **S0** and **S1** to the solution of $A\beta$, residues E11 and H13 did not shift as much as DMSO alone suggesting these compounds may compete for contacts with the peptide although direct comparison is difficult to discern because of the possibility of compounds interacting both with the peptide and/or counteracting the DMSO effect (Supporting Information, Figure S3). With the consideration of the DMSO effect on the $A\beta$ monomer, **S0** and **S1** showed a different ability to recognize $A\beta$ under these conditions compared to the bifunctional compounds **L1-a** and **L1-b**. Contrasting **L1-a** and **L1-b** from **S0** and **S1**, the dimethylamino functionality may not be solely responsible for interaction within this molecular scaffold. The combination of placing two nitrogen atoms into the stilbene framework with the dimethylamino group revealed that minor changes in chemical structure might better control $A\beta$ interaction via hydrogen bonding and hydrophobic contacts. From the compounds investigated, the choice of molecular scaffold and functionality are important variables in selecting effective $A\beta$ interacting molecules to be used as a basis for rational structure-based design. Overall, along with metal binding studies, our NMR investigations above suggest that the bifunctional stilbene derivatives can interact with both metal ions and $A\beta$ demonstrating their bifunctionality.

Docking Studies of L1-a, L1-b, S0, and S1 with $A\beta$. While the residue-specific influence of our compounds (**L1-a** and **L1-b**) on the $A\beta$ monomer was determined by 2D NMR spectroscopy, visualization of the structural details of their contact modes with the peptide backbone or residue side chains would provide more insights into the structure-interaction relationship between small molecules and the peptide. To consider possible conformations of our compounds with $A\beta$, docking studies were conducted using AutoDock4.[38,51−53] A previously determined solution NMR structure of $A\beta_{1-40}$ in SDS micelles (PDB 1BA4) was chosen, and the molecules were evaluated with 10 conformations of $A\beta$.[54] Among them, five conformations of $A\beta$ docked with **L1-a** and **L1-b** were consistent with our NMR results. Based on the lowest energy clusters with highest occurrence, the conformations of compounds with $A\beta$ were selected (Supporting Information, Table S2).

In agreement with NMR observations discussed above, the overall docking results suggested that our bifunctional small molecules may contact the N-terminal region and inner helix of the peptide near the proposed metal binding site (Figure 4 and Supporting Information, Figure S4).[47,54] Most of the conformations presented that the compounds were oriented closer to the hydrophilic metal binding region while one conformation showed ligands docked near the hydrophobic inner helix (conformation C, Supporting Information, Figure S4). The docking results for **L1-a** and **L1-b** illustrated similar binding in three of the conformations analyzed, suggesting that these

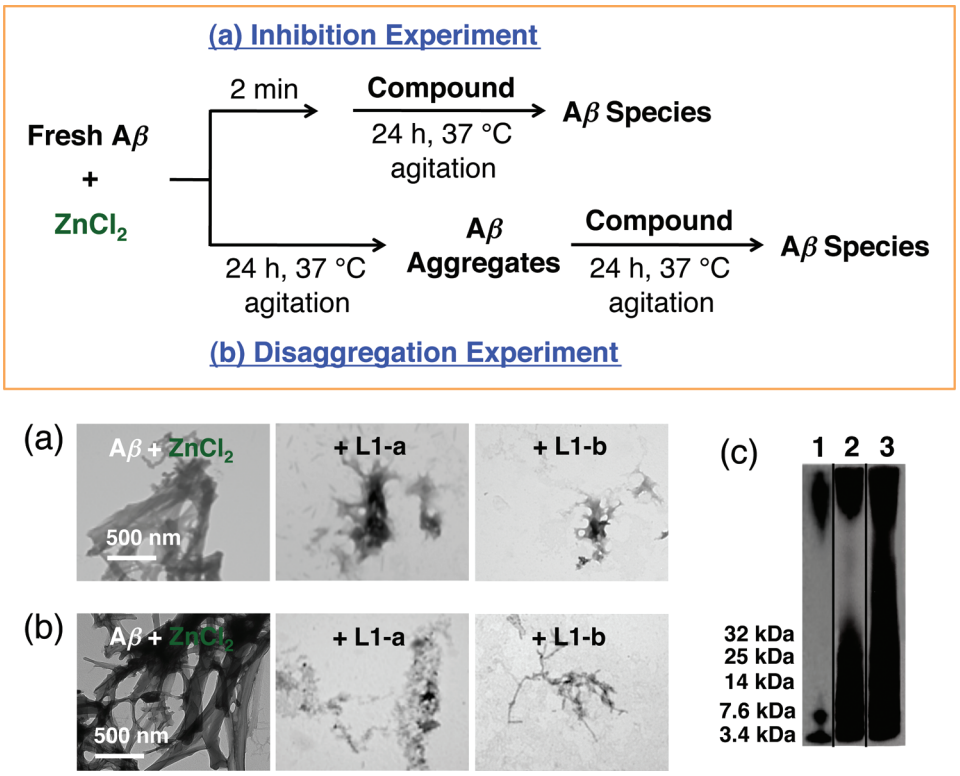

Figure 5. Control of Zn^{2+}-induced Aβ aggregation by small molecules. Top: Scheme of the inhibition and disaggregation experiments. Bottom: TEM images of samples (a) from the inhibition experiment [fresh Aβ treated with $ZnCl_2$ followed by incubation with the compounds (**L1-a** and **L1-b**)]; (b) from the disaggregation experiment [Zn^{2+}-induced Aβ aggregates by 24 h incubation and subsequent 24 h treatment with **L1-a** or **L1-b**]. (c) Results of (a) visualized by native gel electrophoresis followed by Western blot (anti-Aβ antibody 6E10): (**1**) [Aβ + $ZnCl_2$]; (**2**) [**1** + **L1-a**]; (**3**) [**1** + **L1-b**]. Conditions: [Aβ] = 25 μM, [$ZnCl_2$] = 25 μM, [compound] = 50 μM, pH 7.4, 24 h, 37 °C, constant agitation.

molecules may behave similarly with common hydrogen bonding contacts with the peptide backbone and side chain residues. Along with hydrogen bonding interaction, positioning of the dimethylamino group of **L1-b** either toward the hydrophilic N-terminal region or the hydrophobic helical region revealed various amphiphilic contacts with the peptide potentially accounting for the greater chemical shift changes exhibited in the NMR experiment. For **S0** and **S1**, interactions were indicated in the hydrophilic turn and along the inner helix of the peptide as well. More variation between these two molecules (**S0**/**S1**) was observed in the different conformations tested although some conformations showed similar binding modes of these compounds as were seen for **L1-a** and **L1-b** (Figure 4 and Supporting Information, Figure S4).

Different orientations of **L1-a**, **L1-b**, **S0**, and **S1** were visible in the docking investigations, with general interaction near the turn of the peptide (near the metal binding site and inner helix) indicating the utility of the stilbene framework for recognizing the Aβ peptide (Figure 4 and Supporting Information, Figure S4). The individual differences between the ligands docked to the Aβ conformations displayed several possible contacts that may exist in solution, such as hydrogen bonding and hydrophobic contacts that along with NMR imply more favorable interaction of **L1-a** and **L1-b** over **S0** and **S1** with the Aβ peptide. Therefore, these docking results give further support for direct Aβ interaction of our bifunctional small molecules in addition to the NMR investigations.

Effect of L1-a and L1-b on Metal-Induced Aβ Aggregation. The regulation of **L1-a** and **L1-b** on metal-associated Aβ aggregation processes was investigated by TEM and native gel electrophoresis followed by Western blotting using anti-Aβ antibody 6E10.[37−39,55−58] Both inhibition and disaggregation studies were carried out (forward and backward reactions as shown in Figure 5 and Supporting Information, Figure S5). For inhibition experiments, fresh Aβ (25 μM) and $CuCl_2$ or $ZnCl_2$ (25 μM) were treated with the compounds (50 μM) for 24 h (Figure 5 and Supporting Information, Figure S5a). In the disaggregation experiments, the samples containing Aβ and metal chloride salts were incubated for 24 h to allow Aβ aggregates to form, and then agitated with each compound for 24 h (Figure 5 and Supporting Information, Figure S5a).

The presence of metal ions (Cu^{2+} or Zn^{2+}) triggered the formation of large, aggregated Aβ species (Figure 5 and Supporting Information, Figure S5a). On the other hand, upon treatment with our compounds, metal-induced Aβ aggregation was noticeably inhibited according to TEM and native gel analysis.[37−39,58] As shown in Figure 5, Aβ species that had low MW (≤32 kDa) and could enter the gel matrix were visible when our bifunctional compounds were introduced into metal-treated Aβ samples. In particular, much less metal-mediated Aβ aggregation was seen with **L1-b** over **L1-a**. Based on our previous report, at the same conditions, the traditional metal chelators CQ, phen (Figure 1), and EDTA resulted in the generation of high MW Aβ aggregates, which was observed by the same methods.[37,38] The control molecule (**S1**) that does not contain a metal binding site did not block metal-induced Aβ aggregation,[37,38] suggesting that disruption of metal-Aβ interaction was one of the important parameters to block metal-mediated Aβ aggregation with our bifunctional compounds. In addition, the effect of **L1-b** on the metal-free Aβ

dx.doi.org/10.1021/ic2012205 |*Inorg. Chem.* 2011, 50, 10724–10734

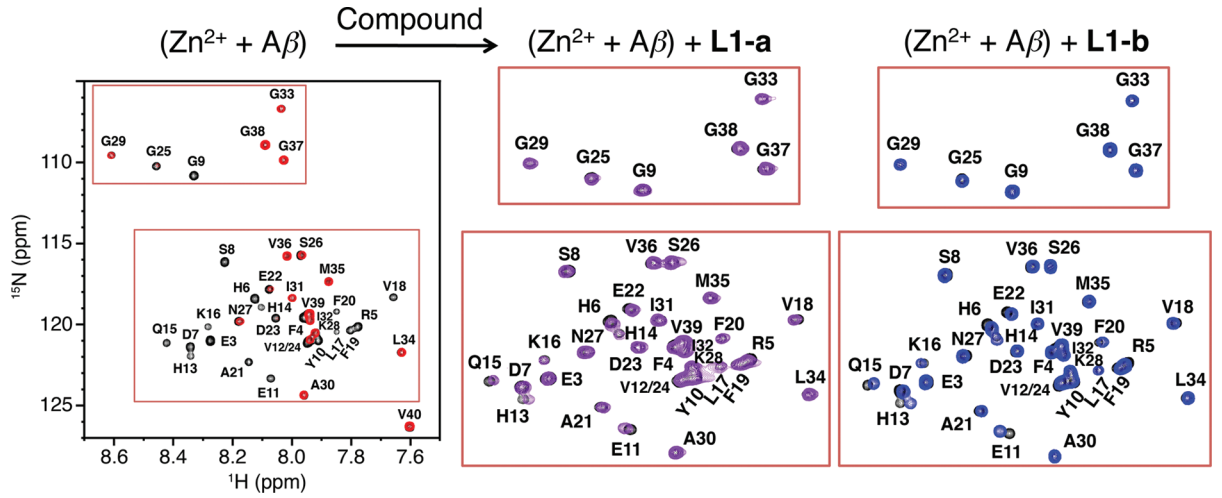

Figure 6. An NMR investigation of **L1-a** and **L1-b** interacting with Zn^{2+}-bound $A\beta_{1-40}$. 2D ^{1}H-^{15}N TROSY-HSQC NMR spectra (900 MHz, 200 mM SDS-d_{25}, 20 mM sodium phosphate, pH 7.3, 7% D_2O (v/v), 25 °C) of ^{15}N-labeled Aβ peptide (ca. 308 μM, black) and upon the addition of $ZnCl_2$ (ca. 1 equiv, red) followed by the addition of 10 equiv of either **L1-a** (purple) or **L1-b** (blue) after 1 h incubation.

aggregation was studied (Supporting Information, Figure S5b). No apparent control of Aβ aggregation by **L1-b** was observed under the metal-free condition, implying that the reactivity of **L1-b** is specific for metal-Aβ species over metal-free Aβ species. Taken together, TEM and Western blot results suggest that the bifunctional molecules could prevent metal-induced Aβ fibrillogenesis generating smaller sized Aβ species more effectively than with traditional metal chelating agents. Therefore, inhibition studies demonstrate that our bifunctional small molecules could function as modulators of metal-induced Aβ aggregate formation, which supports the hypothesis that metal ions could play important roles in Aβ aggregation in AD.

The ability of **L1-a** and **L1-b** to disassemble preformed metal-mediated Aβ aggregates was also explored. Both compounds **L1-a** and **L1-b** were able to alter the structure of metal-triggered Aβ aggregates affording their disaggregation (Figure 5 and Supporting Information, Figure S5).[37] Similar to the inhibition study, **L1-b** provided greater effect toward disaggregation of preformed metal-Aβ aggregates than **L1-a**. Different from the bifunctional molecules, our previous studies showed that the traditional metal chelators phen and EDTA did not disaggregate preformed metal-associated Aβ aggregates, though changes in morphology were observed.[37,38,55] In the case of CQ, partial disaggregation of Zn^{2+}-treated Aβ aggregates was recorded.[55] Therefore, on the basis of the results from both inhibition and disaggregation experiments, our bifunctional molecules **L1-a** and **L1-b** were better able to control metal-mediated Aβ aggregation processes (formation of metal-induced Aβ aggregates as well as their disaggregation) than the traditional metal chelators. The compound **L1-b** that indicated greater bifunctionality (vide supra) exhibited more effective control of metal-induced Aβ aggregation, compared to **L1-a**. These observations imply that the bifunctionality of our compounds leads to enhanced reactivity with metal-Aβ species (structure-interaction-reactivity relationship).

Investigation of the Reaction of Zn^{2+}-Treated Aβ with L1-a and L1-b. To understand possible mechanisms underlying the modulation of metal-triggered Aβ events by our small molecules, spectroscopic investigations were conducted using high-resolution 2D NMR and UV−vis on Zn^{2+}-treated Aβ solutions in the absence and presence of compounds. To first determine the ability of **L1-b** to compete for Zn^{2+} binding from Aβ, the compound (40 μM) was added to a solution containing equal concentrations of $ZnCl_2$ and Aβ (20 μM, 200 mM SDS, 20 mM sodium phosphate buffer, pH 7.3). The resulting UV−vis spectrum showed the generation of Zn^{2+}-**L1-b** species with optical bands near 450 nm, which is comparable to those from only the metal−ligand complex (Supporting Information, Figure S6a). Because of the small optical change upon addition of Zn^{2+} into the solution of **L1-a** (Supporting Information, Figure S1), the UV−vis study of Aβ, Zn^{2+}, and **L1-a** was not performed. Carrying out 2D TROSY-HSQC experiments under similar conditions suggested that more than simple metal chelation by our small molecules from the peptide may occur. As expected from previous reports, addition of 1 equiv of $ZnCl_2$ to an NMR solution of Aβ (308 μM, 200 mM SDS-d_{25}, 20 mM sodium phosphate buffer, pH 7.3, 7% D_2O (v/v), 25 °C) caused a large portion of the 2D NMR spectrum to disappear because of line broadening as a result of Zn^{2+} binding (Figure 6).[20,69,70] With the treatment of 10 equiv of compounds, the ^{1}H and ^{15}N cross peaks absent upon introduction of Zn^{2+} were recovered with 30 min incubation of **L1-a** and **L1-b** (Figure 6). Additionally, cross peak shifts were observed for both **L1-a** and **L1-b** that indicated small variations from the metal free samples in the N-terminal and inner helix portions of the peptide (Figure 6 and Supporting Information, Figure S6b). These observations suggest that the interaction of these bifunctional molecules with Zn^{2+}-Aβ occurs via a combination of metal chelation by the compound from Aβ and interaction of free compound and/or the metal complex with Aβ.[38] Metal chelation was also supported by optical spectra indicating Zn^{2+} binding to the compound (Supporting Information, Figure S6a) as discussed above.

Based on reactivity studies of compounds with metal-Aβ species by TEM (vide supra), disruption of both metal-peptide and peptide−peptide interactions could be a driving force for preventing metal-induced Aβ aggregation. From previously reported NMR observations, the traditional metal chelator EDTA was shown to remove Cu^{2+} or Zn^{2+} from Aβ;[71] but from our previously reported TEM results discussed above, EDTA and other orthodox metal chelators did not deter metal-induced Aβ aggregation.[37,38] Our NMR and optical results involving

dx.doi.org/10.1021/ic2012205 |Inorg. Chem. 2011, 50, 10724–10734

Zn^{2+}-Aβ species and compounds indicated that the observed interference on metal-Aβ reactivity could be due to the removal of the metal ion from metal-Aβ species (through metal chelation by the ligand or ligand-induced metal-Aβ conformational changes) and/or the potential formation of ternary type complexes involving Aβ, Zn^{2+}, and compound (through the interaction of ligand with metal-Aβ species or ligand−metal complexes with the peptide).[38] Thus, small variations in the stilbene scaffold could not only affect ligand binding to Aβ but also indicate the ability to tune interactions with metal-Aβ species.

Regulation of Cu-Aβ-Induced ROS Production by L1-a and L1-b. The production of ROS by redox active metal-Aβ species and subsequent oxidative stress may lead to neurotoxicity in AD.[2,5,10−17,21−25] In addition to targeting metal-Aβ species for modulating their aggregation properties, control of ROS formation by our bifunctional small molecules must be considered. Employing the HRP/Amplex Red assay,[23,32,37,38,40] amounts of H_2O_2 produced by Cu-Aβ species in the absence and presence of our bifunctional molecules (**L1-a** and **L1-b**) was determined. Inhibition of Cu-Aβ-triggered H_2O_2 formation by **L1-a** and **L1-b** was observed (reduction of H_2O_2 formation by 64(±1.1)% (for **L1-a**) and 70(±0.75)% (for **L1-b**)[37]). Other metal chelating agents CQ and EDTA also exhibited decreased H_2O_2 production under the same conditions.[37,38] In the absence of Aβ, free Cu ions generated about 94% of the amount of H_2O_2 as was produced in the presence of the peptide. The ligands were also able to lower the level of H_2O_2 generated by peptide-free Cu by about 52% for **L1-a** and 56% for **L1-b** ([$CuCl_2$]/[ligand] = 1:2), relative to Cu-Aβ. Taken together, the prevention of H_2O_2 formation by peptide-free or -bound Cu in vitro by our stilbene derivatives was observed, which may suggest their use as ROS regulators.

Cytotoxicity of L1-a and L1-b with and without Metal Chloride Salts As Well As Their Ability to Modulate Metal-Aβ Neurotoxicity in Human Neuroblastoma Cells. First, cell viability in the presence of our compounds at various concentrations was evaluated in human neuroblastoma M17 and AS cells after 24 or 72 h incubation. The cell survival rates were monitored by the MTT assay.[37,38] After 24 h of incubation with our bifunctional small molecules, no toxic effects were observed in either M17 or AS cells. After 72 h, cytotoxicity of **L1-a** was not visible up to 100 μM for either cell line. For both cell lines (M17/AS), **L1-b** (up to 100 μM) showed 66(±3.2)/84(±4.2)% survival, respectively (Supporting Information, Figure S7a). Considering the previously studied cell viability of CQ and phen (30(±0.3)/34(±0.8)% and 37(±0.5)/44(±0.2)% in M17 and AS cell lines, respectively),[38] toxicity of our compounds may be minimal up to 100 μM. Furthermore, the cytotoxicity of **L1-a** and **L1-b** with $CuCl_2$ or $ZnCl_2$ (5−120 μM) at 1:1 and 1:2 metal/compound ratios for 24 h was examined in the M17 cell line. Cell survival (ca. 96−100%) was observed from cells treated with up to 20 μM $CuCl_2$ or $ZnCl_2$ and 20/40 μM compounds (Supporting Information, Figures S7b and S7c). Above 40 μM metal chloride salt and 40/80 μM compounds, the cell viability decreased. When $CuCl_2$ or $ZnCl_2$, (120 μM) and compounds (**L1-a** or **L1-b**; 120 or 240 μM) were incubated with cells, about 40−50% cell survival was indicated. From these cytotoxicity studies, our bifunctional small molecules were minimally toxic at concentrations of 40 μM or lower in the presence of up to 20 μM metal ions. Thus, based on these cytotoxicity studies, testing our compounds' effect on metal-Aβ species in a cellular environment could be explored.

To investigate how our bifunctional molecules influence the neurotoxicity induced by metal-associated Aβ species, we carried out the reactions of metal ions, Aβ, and compounds in the human neuroblastoma M17 cell line.[37,38] Our cell studies presented 70(±2.4) or 80(±4.3)% of cells survived upon 24 h incubation with Cu^{2+}- or Zn^{2+}-treated Aβ (Figure 7). Interestingly, as described in Figure 7, when the compound with the dimethylamino functionality (**L1-b**) was added to Cu^{2+}- and Zn^{2+}-Aβ-treated cells, cell survival rates increased to about 90[37] and 100%, respectively. Compared to **L1-b**, **L1-a** induced a slight increase in the survival of cells treated with Cu^{2+}- or Zn^{2+}-treated Aβ (77% and 86% cell viability for the samples of Cu^{2+} and Zn^{2+}, respectively). Under the same conditions traditional metal chelators such as CQ, EDTA, and phen were not able to recover the cell survival from metal-Aβ neurotoxicity.[37,38] Overall, these cell-based studies employing our bifunctional compounds demonstrate their capability to regulate metal-Aβ neurotoxicity in living cells, which is expected based on their reactivity in vitro (anti-Aβ aggregation as well as ROS regulation). These cell studies also agree with the overall observation that assessing the ability of our bifunctional compounds to interact with metal-Aβ species is a key factor to comprehend greater reactivity toward metal-induced Aβ events (structure-interaction-reactivity relationship).

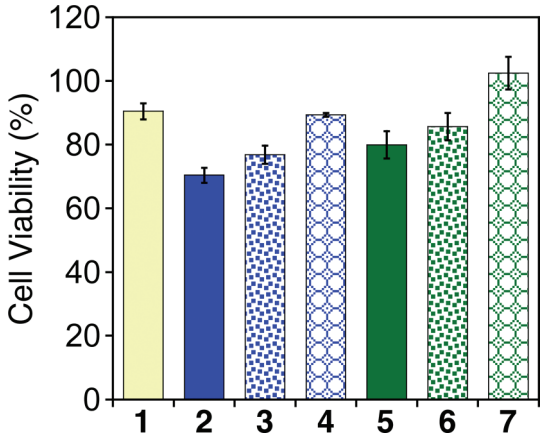

Figure 7. Regulation of metal-associated Aβ neurotoxicity in M17 cells for 24 h using the MTT assay. Cell viability (%) upon incubation of (**1**) Aβ; (**2**) [Aβ + $CuCl_2$]; (**3**) [Aβ + $CuCl_2$ + **L1-a**]; (**4**) [Aβ + $CuCl_2$ + **L1-b**]; (**5**) [Aβ + $ZnCl_2$]; (**6**) [Aβ + $ZnCl_2$ + **L1-a**]; (**7**) [Aβ + $ZnCl_2$ + **L1-b**]. Condition: [Aβ] = 20 μM, [$CuCl_2$ or $ZnCl_2$] = 20 μM, [compound] = 40 μM. Cell viability (%) shown in the figure is relative to that of cells containing 1% DMSO (v/v). Cytotoxicity from cells treated with metal ions and compounds were not indicated at this condition (Supporting Information, Figures S7b and S7c).

SUMMARY AND PERSPECTIVE

Small molecules that have the ability to target and modulate metal-Aβ species are greatly desired and could be instrumental in determining how metal-associated pathways may be involved with AD neuropathogenesis. To achieve this, we have taken the rational structure-based design approach to develop bifunctional compounds that are capable of chelating metal ions as well as interacting with Aβ species. Our group has previously applied this strategy to the chemical structures of two known Aβ aggregate indicators, *p*-I-stilbene and IMPY, that were altered through installation of heteroatoms for metal coordination. These small, neutral, lipophilic imaging agents have demonstrated attributes that render them beneficial for this application.

According to the promising behavior of our first series of compounds, a further generation based on the same frameworks was devised. Importantly, the entire structure was likely a valuable contribution to targeting Aβ while simple structural modifications could improve their interaction and reactivity with Aβ and metal-Aβ species. Here, we focus on two compounds that serve as an extension to our previous studies of stilbene-like molecules; these studies supplement our understanding of how simple modifications such as the inclusion of two nitrogen atoms for metal chelation and the presence or absence of the dimethylamino functionality can influence interaction/reactivity. The bifunctionality (metal chelation and Aβ interaction) of the compounds (**L1-a** and **L1-b**) was verified by spectroscopic and other methods including UV−vis, high-resolution 2D NMR, and X-ray crystallography. Further biochemical studies displayed the potential direct interaction of our small molecules with metal-Aβ species through their ability to regulate reactivity (metal-induced Aβ aggregation and neurotoxicity) in vitro and in living cells. Together with our previous work, the studies presented here validate the selection of the stilbene compound as a model interaction framework as it importantly interacts with Aβ peptides in various aggregated forms and displays minimal toxicity in human neuroblastoma cells. In our studies, the structural moieties, such as dimethylamino functionality, are crucial parameters for a structure-interaction-reactivity relationship that can be applied to develop and tune small molecules that can target metal-Aβ species allowing for anti-Aβ aggregation, ROS regulation, and modulation of metal-Aβ neurotoxicity. Continuing investigations on this theme will be conducted to advance the construction and study of suitable chemical tools for understanding metal-Aβ-involved processes in chemistry and biology as well as potential therapeutic agents for AD.

■ ASSOCIATED CONTENT

Supporting Information. Tables S1 and S2, Figures S1−S7, as well as X-ray crystallographic file (CIF file). This material is available free of charge via the Internet at http://pubs.acs.org.

■ AUTHOR INFORMATION

Corresponding Author
*E-mail: mhlim@umich.edu.

■ ACKNOWLEDGMENT

This work was supported by start-up funding from the University of Michigan, the Alzheimer's Art Quilt Initiative (AAQI), as well as the Alzheimer's Association (NIRG-10-172326) (to M.H.L.) and NIH (DK078885 and RR023597 to A.R.). We acknowledge funding from NSF Grant CHE-0840456 for X-ray instrumentation. J.J.B. is grateful for the Murrill Memorial Scholarship from the Department of Chemistry at the University of Michigan. K.N. conducted this work as an intern from the Western Reserve Academy, OH, U.S.A. and is currently at Hankuk Academy Of Foreign Studies, Korea. We thank Kermit Johnson, Dr. Subramanian Vivekanandan, and Dr. Ravi P. R. Nanga for help with 900 MHz NMR experiments and data analysis, as well as Allana Mancino and Nathan Merrill for experimental assistance.

■ REFERENCES

(1) www.alz.org
(2) Jakob-Roetne, R.; Jacobsen, H. *Angew. Chem., Int. Ed.* **2009**, *48*, 3030–3059.
(3) Hardy, J.; Selkoe, D. J. *Science* **2002**, *297*, 353–356.
(4) Haass, C.; Selkoe, D. J. *Nat. Rev. Mol. Cell Biol.* **2007**, *8*, 101–112.
(5) DeToma, A. S.; Salamekh, S.; Ramamoorthy, A.; Lim, M. H. *Chem. Soc. Rev.* **2012**, DOI: 10.1039/c1cs15112f.
(6) Roychaudhuri, R.; Yang, M.; Hoshi, M. M.; Teplow, D. B. *J. Biol. Chem.* **2009**, *284*, 4749–4753.
(7) Miller, Y.; Ma, B.; Nussinov, R. *Chem. Rev.* **2010**, *110*, 4820–4838.
(8) Lovell, M. A.; Robertson, J. D.; Teesdale, W. J.; Campbell, J. L.; Markesbery, W. R. *J. Neurol. Sci.* **1998**, *158*, 47–52.
(9) Miller, L. M.; Wang, Q.; Telivala, T. P.; Smith, R. J.; Lanzirotti, A.; Miklossy, J. *J. Struct. Biol.* **2006**, *155*, 30–37.
(10) Rauk, A. *Chem. Soc. Rev.* **2009**, *38*, 2698–2715.
(11) Gaggelli, E.; Kozlowski, H.; Valensin, D.; Valensin, G. *Chem. Rev.* **2006**, *106*, 1995–2044.
(12) Zatta, P.; Drago, D.; Bolognin, S.; Sensi, S. L. *Trends Pharmacol. Sci.* **2009**, *30*, 346–355.
(13) Faller, P.; Hureau, C. *Dalton Trans.* **2009**, 1080–1094.
(14) Faller, P. *ChemBioChem* **2009**, *10*, 2837–2845.
(15) Scott, L. E.; Orvig, C. *Chem. Rev.* **2009**, *109*, 4885–4910.
(16) Bush, A. I.; Tanzi, R. E. *Neurotherapeutics* **2008**, *5*, 421–432.
(17) Barnham, K. J.; Curtain, C. C.; Bush, A. I. *Protein Rev.* **2007**, *6*, 31–47.
(18) Karr, J. W.; Kaupp, L. J.; Szalai, V. A. *J. Am. Chem. Soc.* **2004**, *126*, 13534–13538.
(19) Karr, J. W.; Szalai, V. A. *Biochemistry* **2008**, *47*, 5006–5016.
(20) Danielsson, J.; Pierattelli, R.; Banci, L.; Gräslund, A. *FEBS J.* **2007**, *274*, 46–59.
(21) Cappai, R.; Barnham, K. J. *Neurochem. Res.* **2008**, *33*, 526–532.
(22) Zhu, X.; Su, B.; Wang, X.; Smith, M. A.; Perry, G. *Cell. Mol. Life Sci.* **2007**, *64*, 2202–2210.
(23) Hureau, C.; Faller, P. *Biochimie* **2009**, *91*, 1212–1217.
(24) Molina-Holgado, F.; Hider, R. C.; Gaeta, A.; Williams, R.; Francis, P. *BioMetals* **2007**, *20*, 639–654.
(25) Huang, X.; Moir, R. D.; Tanzi, R. E.; Bush, A. I.; Rogers, J. T. *Ann. N.Y. Acad. Sci.* **2004**, *1012*, 153–163.
(26) Cherny, R. A.; Atwood, C. S.; Xilinas, M. E.; Gray, D. N.; Jones, W. D.; McLean, C. A.; Barnham, K. J.; Volitakis, I.; Fraser, F. W.; Kim, Y.; Huang, X.; Goldstein, L. E.; Moir, R. D.; Lim, J. T.; Beyreuther, K.; Zheng, H.; Tanzi, R. E.; Masters, C. L.; Bush, A. I. *Neuron* **2001**, *30*, 665–676.
(27) Adlard, P. A.; Cherny, R. A.; Finkelstein, D. I.; Gautier, E.; Robb, E.; Cortes, M.; Volitakis, I.; Liu, X.; Smith, J. P.; Perez, K.; Laughton, K.; Li, Q.-X.; Charman, S. A.; Nicolazzo, J. A.; Wilkins, S.; Deleva, K.; Lynch, T.; Kok, G.; Ritchie, C. W.; Tanzi, R. E.; Cappai, R.; Masters, C. L.; Barnham, K. J.; Bush, A. I. *Neuron* **2008**, *59*, 43–55.
(28) Perez, L. R.; Franz, K. J. *Dalton Trans.* **2010**, *39*, 2177–2187.
(29) Dickens, M. G.; Franz, K. J. *ChemBioChem* **2010**, *11*, 59–62.
(30) Boldron, C.; Van der Auwera, I.; Deraeve, C.; Gornitzka, H.; Wera, S.; Pitié, M.; Van Leuven, F.; Meunier, B. *ChemBioChem* **2005**, *6*, 1976–1980.
(31) Deraeve, C.; Boldron, C.; Maraval, A.; Mazarguil, H.; Gornitzka, H.; Vendier, L.; Pitié, M.; Meunier, B. *Chem.—Eur. J.* **2008**, *14*, 682–696.
(32) Deraeve, C.; Pitie, M.; Meunier, B. *J. Inorg. Biochem.* **2006**, *100*, 2117–2126.
(33) Hureau, C.; Sasaki, I.; Gras, E.; Faller, P. *ChemBioChem* **2010**, *11*, 950–953.
(34) Braymer, J. J.; DeToma, A. S.; Choi, J.-S.; Ko, K. S.; Lim, M. H. *Int. J. Alzheimers Dis.* **2011**, *2011*, 623051.
(35) Dedeoglu, A.; Cormier, K.; Payton, S.; Tseitlin, K. A.; Kremsky, J. N.; Lai, L.; Li, X.; Moir, R. D.; Tanzi, R. E.; Bush, A. I.; Kowall, N. W.; Rogers, J. T.; Huang, X. *Exp. Gerontol.* **2004**, *39*, 1641–1649.
(36) Rodríguez-Rodríguez, C.; Sánchez de Groot, N.; Rimola, A.; Álvarez-Larena, Á.; Lloveras, V.; Vidal-Gancedo, J.; Ventura, S.; Vendrell, J.; Sodupe, M.; González-Duarte, P. *J. Am. Chem. Soc.* **2009**, *131*, 1436–1451.

(37) Hindo, S. S.; Mancino, A. M.; Braymer, J. J.; Liu, Y.; Vivekanandan, S.; Ramamoorthy, A.; Lim, M. H. *J. Am. Chem. Soc.* **2009**, *131*, 16663–16665.
(38) Choi, J.-S.; Braymer, J. J.; Nanga, R. P. R.; Ramamoorthy, A.; Lim, M. H. *Proc. Natl. Acad. Sci. U.S.A.* **2010**, *107*, 21990–21995.
(39) Choi, J.-S.; Braymer, J. J.; Park, S. K.; Mustafa, S.; Chae, J.; Lim, M. H. *Metallomics* **2011**, *3*, 284–291.
(40) Himes, R. A.; Park, G. Y.; Siluvai, G. S.; Blackburn, N. J.; Karlin, K. D. *Angew. Chem., Int. Ed.* **2008**, *47*, 9084–9087.
(41) Sheldrick, G. M. *SADABS or TWINABS, Program for Empirical Absorption Correction of Area Detector Data*, version 2008/1; Bruker AXA: Madison, WI, 2008.
(42) *SAINTPLUS: Software for the CCD Detector System*, version 7.60a ed.; Bruker AXA: Madison, WI, 2009.
(43) Sheldrick, G. *SHELXTL*, version 2008/3rd ed.; Bruker AXA: Madison, WI, 2008.
(44) Spek, A. L. PLATON, A. *Multipurpose Crystallographic Tool*; Utrecht University: Utrecht, The Netherlands, 2010.
(45) Sheldrick, G. M. *CELL_NOW, Program for Indexing Twins and Other Problem Crystals*, version 2008/2; University of Göttingen: Göttingen, Germany, 2008.
(46) Because of low solubility of the **S0** and **S1** in the NMR solvent, they were added from a stock solution prepared in DMSO-d_6.
(47) Jarvet, J.; Danielsson, J.; Damberg, P.; Oleszczuk, M.; Gräslund, A. *J. Biomol. NMR* **2007**, *39*, 63–72.
(48) Grzesiek, S.; Bax, A.; Clore, G. M.; Gronenborn, A. M.; Hu, J. S.; Kaufman, J.; Palmer, I.; Stahl, S. J.; Wingfield, P. T. *Nat. Struct. Biol.* **1996**, *3*, 340–345.
(49) Garrett, D. S.; Seok, Y.-J.; Peterkofsky, A.; Clore, G. M.; Gronenborn, A. M. *Biochemistry* **1997**, *36*, 4393–4398.
(50) Foster, M. P.; Wuttke, D. S.; Clemens, K. R.; Jahnke, W.; Radhakrishnan, I.; Tennant, L.; Reymond, M.; Chung, J.; Wright, P. E. *J. Biomol. NMR* **1998**, *12*, 51–71.
(51) Morris, G. M.; Goodsell, D. S.; Halliday, R. S.; Huey, R.; Hart, W. E.; Belew, R. K.; Olson, A. J. *J. Comput. Chem.* **1998**, *19*, 1639–1662.
(52) Morris, G. M.; Huey, R.; Lindstrom, W.; Sanner, M. F.; Belew, R. K.; Goodsell, D. S.; Olson, A. J. *J. Comput. Chem.* **2009**, *30*, 2785–2791.
(53) Morris, G. M.; Huey, R.; Olson, A. I. *Curr. Protoc. Bioinf.* **2008**, *Chapter 8*, 8.14.11–18.14.40.
(54) Coles, M.; Bicknell, W.; Watson, A. A.; Fairlie, D. P.; Craik, D. J. *Biochemistry* **1998**, *37*, 11064–11077.
(55) Mancino, A. M.; Hindo, S. S.; Kochi, A.; Lim, M. H. *Inorg. Chem.* **2009**, *48*, 9596–9598.
(56) Nielsen, E. H.; Nybo, M.; Svehag, S.-E. *Methods Enzymol.* **1999**, *309*, 491–496.
(57) Reinke, A. A.; Seh, H. Y.; Gestwicki, J. E. *Bioorg. Med. Chem. Lett.* **2009**, *19*, 4952–4957.
(58) DeToma, A. S.; Choi, J.-S.; Braymer, J. J.; Lim, M. H. *ChemBioChem* **2011**, *12*, 1198–1201.
(59) Leuma Yona, R.; Mazères, S.; Faller, P.; Gras, E. *ChemMedChem* **2008**, *3*, 63–66.
(60) Ono, M.; Yoshida, N.; Ishibashi, K.; Haratake, M.; Arano, Y.; Mori, H.; Nakayama, M. *J. Med. Chem.* **2005**, *48*, 7253–7260.
(61) Bloom, S. M.; Borror, A. L.; Greenwald, R. B.; Vol. U.S. Patent 4,006,151, 1977.
(62) The ligands (**L1-a** and **L1-b**) have limited stability in aqueous solutions ($t_{1/2}$ = ca. 70 s and ca. 240 s for **L1-a** and **L1-b**, respectively, in 20 mM HEPES buffer (pH 7.4) containing 150 mM NaCl ([ligand] = 40 μM)) because of their hydrolysis, which was confirmed by MS. The stability of the two compounds was enhanced in the presence of metal ions (two- or three-fold increase in $t_{1/2}$ with $CuCl_2$ or $ZnCl_2$). On the basis of the stability studies of the ligands, the hydrolyzed products may contribute to metal-Aβ reactivity.
(63) Dehghanpour, S.; Mahmoudi, A.; Khalaj, M.; Salmanpour, S.; Adib, M. *Acta Crystallogr., Sect. E: Struct. Rep. Online* **2007**, *63*, m2841.
(64) Shao, H.; Jao, S.; Ma, K.; Zagorski, M. G. *J. Mol. Biol.* **1999**, *285*, 755–773.
(65) Shankar, G. M.; Li, S.; Mehta, T. H.; Garcia-Munoz, A.; Shepardson, N. E.; Smith, I.; Brett, F. M.; Farrell, M. A.; Rowan, M. J.; Lemere, C. A.; Regan, C. M.; Walsh, D. M.; Sabatini, B. L.; Selkoe, D. J. *Nat. Med.* **2008**, *14*, 837–842.
(66) Butterfield, S. M.; Lashuel, H. A. *Angew. Chem., Int. Ed.* **2010**, *49*, 5628–5654.
(67) Jarvet, J.; Damberg, P.; Danielsson, J.; Johansson, I.; Eriksson, L. E. G.; Gräslund, A. *FEBS Lett.* **2003**, *555*, 371–374.
(68) Walsh, D. M.; Hartley, D. M.; Kusumoto, Y.; Fezoui, Y.; Condron, M. M.; Lomakin, A.; Benedek, G. B.; Selkoe, D. J.; Teplow, D. B. *J. Biol. Chem.* **1999**, *274*, 25945–25952.
(69) Syme, C. D.; Viles, J. H. *Biochim. Biophys. Acta, Proteins Proteomics* **2006**, *1764*, 246–256.
(70) Gaggelli, E.; Janicka-Klos, A.; Jankowska, E.; Kozlowski, H.; Migliorini, C.; Molteni, E.; Valensin, D.; Valensin, G.; Wieczerzak, E. *J. Phys. Chem. B* **2008**, *112*, 100–109.
(71) Hou, L.; Zagorski, M. G. *J. Am. Chem. Soc.* **2006**, *128*, 9260–9261.